International Conference on Space Optics—ICSO 2006

Noordwijk, Netherlands

27–30 June 2006

Edited by Errico Armandillo, Josiane Costeraste, and Nikos Karafolas

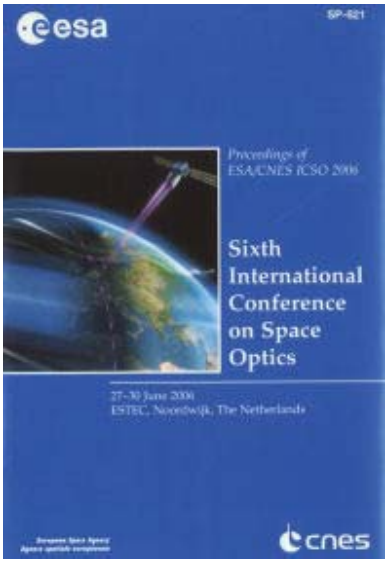

Synthetic aperture co-phasing and co-alignment using an external reference source

Stéphane Roose, Jean-Christophe Bolsee, Jean-Hervé Lecat, Nicolas Loix

International Conference on Space Optics — ICSO 2006, edited by Errico Armandillo, Josiane Costeraste, Nikos Karafolas, Proc. of SPIE Vol. 10567, 105670A · © 2006 ESA and CNES
CCC code: 0277-786X/17/$18 · doi: 10.1117/12.2308074

SYNTHETIC APERTURE CO-PHASING AND CO-ALIGNMENT USING AN EXTERNAL REFERENCE SOURCE

Stéphane Roose[1], Jean-Christophe Bolsée[1], Jean-Hervé Lecat[1], Nicolas Loix[2]

[1]*Centre Spatial de Liège, Université de Liège,Avenue du Pré-Aily, B-4031 Angleur-Liège, Belgium*
Phone: 32 4 367 66 68 Fax 32 4 367 56 13, sroose@ulg.ac.be
[2]*Micromega Dynamics,Rue des Chasseurs Ardennais, B-4031 Angleur-Liège, Belgium*
Phone: 32 4 365 23 63 Fax 32 4 361 67 45

1. ABSTRACT

A breadboard set-up has demonstrated a concept of co-phasing and co-alignment based on an external reference source for synthetic aperture telescopes applications. These types of systems can be extremely valuable in order to perform coarse re-alignment of synthetic aperture telescope, following thermo-elastic deformation and deployment effects in space flight environments.

2. INTRODUCTION

Synthetic aperture optics applied to space optics applications, is growing in importance. Recent technologic developments have been undertaken for astronomic missions like DARWIN. In the field of Earth observation one is still looking at a best match between applications, missions, deployment strategies and co-phasing technology. Some pioneering studies have already been pursued in that field [1][2][3]. Among different strategies to co-phase and co-align an array of telescopes or petals there are techniques which use the image information to retrieve the misalignment contributions. Other techniques measure directly optical path and angular differences with metrology using an internal reference source to the system.

In the present communication, we have worked out a concept of sensor, which allows co-phasing and co-aligning multiple apertures with an incoherent white light point from the observation scene. It is an absolute reference source external to the system. This conceptual approach has been implemented in a breadboard set-up. The set-up had also the ambition to make a closed loop with a delay line, which allows correction of piston and tilt.

One is obviously aware that the accuracies and resolutions are not of the same order of magnitude obtained with fine laser metrology.

The concept allows performing coarse phasing and alignment [4], and this in order to remove low temporal spatial frequency and large amplitude deformations.

Our discussion will start with a description of the breadboard set-up and its subsystems.

Proc. '6th Internat. Conf. on Space Optics', ESTEC, Noordwijk, The Netherlands, 27-30 June 2006 (ESA SP-621, June 2006)

3. GENERAL LAY-OUT

The co-phasing demonstrator is composed of a source block which simulates the external source, a beam collimator, a mask with two apertures, two delay lines, a piston sensor block and a tip/tilt sensor block and finally a recombining block (Fig. 1, Fig. 2).

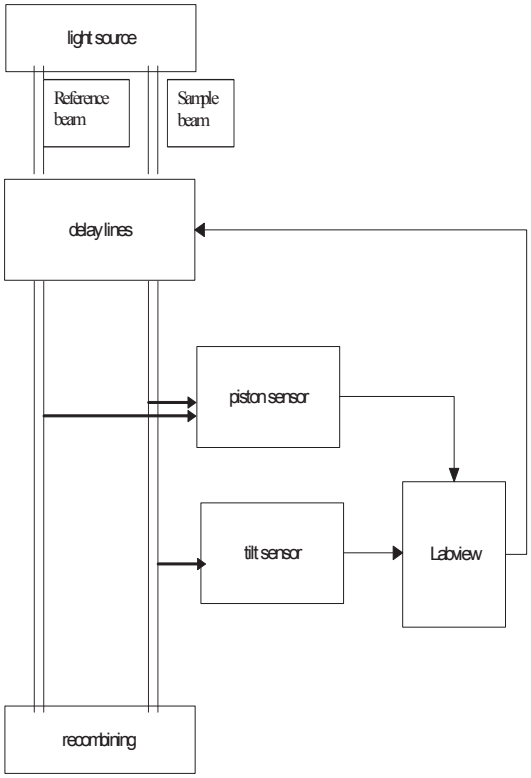

Fig. 1. General configuration.

A light source block provides two white light spatially coherent collimated beams, named reference and sample beams. One of the two beams is delayed and tilted by the optical delay line (sample beam). The two sensors (tip/tilt and piston) measure the perturbation. All the sensor data are sent to a commercial acquisition system. It computes the corrections to be applied to the actuators and this perturbation is compensated in real time by the delay lines actuators.

4. EXTERNAL SOURCE

The source is a XENON source. A part of the beam is focussed on a pinhole (10 μm) and re-collimated with a singlet lens. This point simulates for example a point on the Earth.
The piston sensor uses a part of the spectrum between 800 nm and 900 nm. This part of the spectrum is extracted with two dichroic mirrors. Strong spectral lines in this part of the spectrum make the use of the full 100 nm span impractical, due to large intensity differences. One will effectively work between 879 nm – 886 nm.
The synthetic aperture is created by putting a mask in the collimated beam.

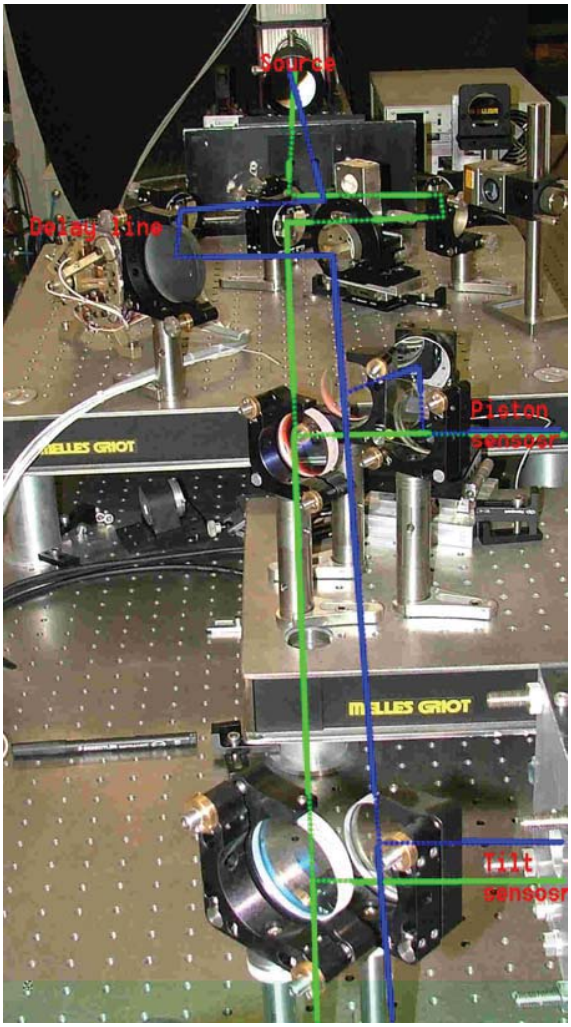

Fig. 2. Picture of the integrated hardware.

5. THE DELAY LINE

The active element of the delay line is build by MICROMEGA DYNAMICS (Fig. 3).

The guiding mechanism of the delay line is based on magnetic bearings. Driven through a dedicated controller, the magnetic bearing behaves like a sophisticated one degree of freedom contact-less spring-damper system. The configuration retained is based on a decentralized control approach. Each actuator is driven by its own controller, associated to a collocated sensor, which is an "Eddy Current" type.

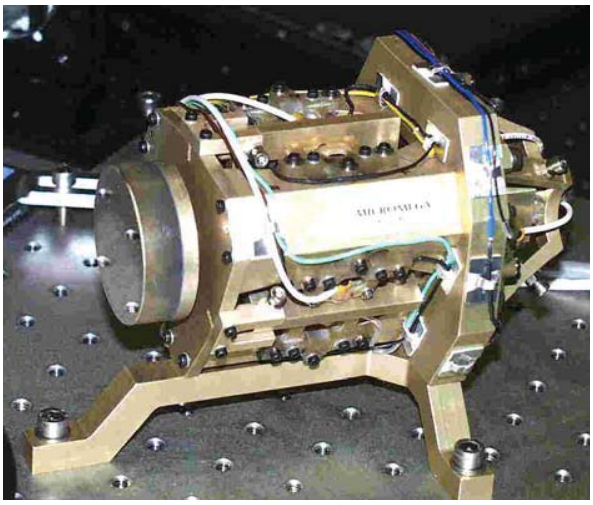

Fig. 3. The piston/tilt actuator.

6. TIP/TILT SENSOR

The external sensor is based on a 0.5 m focal length achromatic lens, which focuses the light on a commercial Position Sensing Device (PSD). Angular movements of the tilt sensor with respect to the collimated beam are recorded as linear displacements on the PSD. The PSD read-out is linear with respect to the angle (Fig. 4).

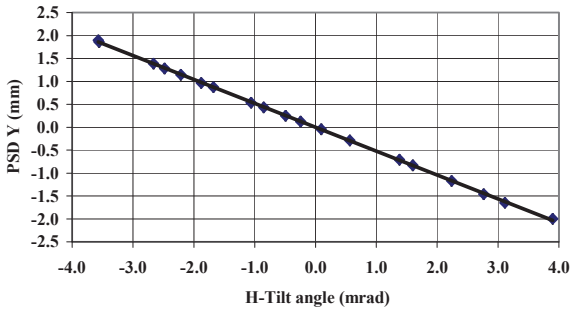

Fig. 4. Tilt sensor linearity.

The precision of the measurement is 0.013 mrad. The absolute accuracy is 0.022 mrad. The open and closed loop range is ±3mrad.
In closed loop, the stability around a set point was investigated. The point spread function (PSF) of one sub-aperture (sample beam) is recorded.

The centre of the PSF is computed with a centroidisation algorithm. The recorded PSF stability corresponds to goal of 0.010 mrad.
The control loop stability is typically 1/10 in RMS of this PSF, and 1/3 in PTV (Peak to Valley).

signal level	SUM=0.6 V		SUM=1.5 V		SUM=1.9 V		SUM=4.8 V	
axis	X	Y	X	Y	X	Y	X	Y
RMS(mrad)	0.012	0.012	0.009	0.009	0.010	0.005	0.013	0.010
PTV(rad)	0.045	0.031	0.045	0.037	0.025	0.025	0.033	0.045

Table 1: Tip/tilt stability analysis of PSF in image plane.

7. PISTON SENSOR

The piston measurement principle is based on interferometry with dispersed light. The beams coming from the telescopes are extracted with two dichroic mirrors, superimposed and spread according their wavelength, forming a spectrum on a linear CCD camera (2048 pixels) (Fig. 6).

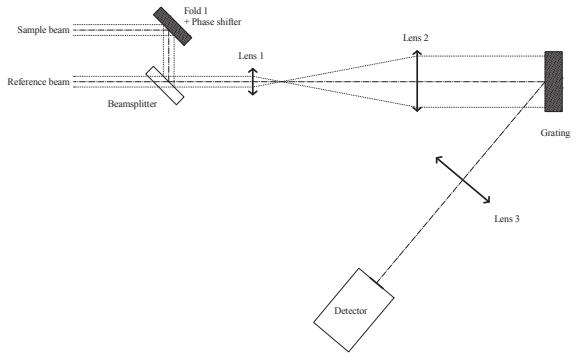

Fig. 5. Piston sensor set-up.

Coherent addition of the wavefront errors caused by piston variations between telescopes results in the intensity modulation of the spectrum (Fig. 6).

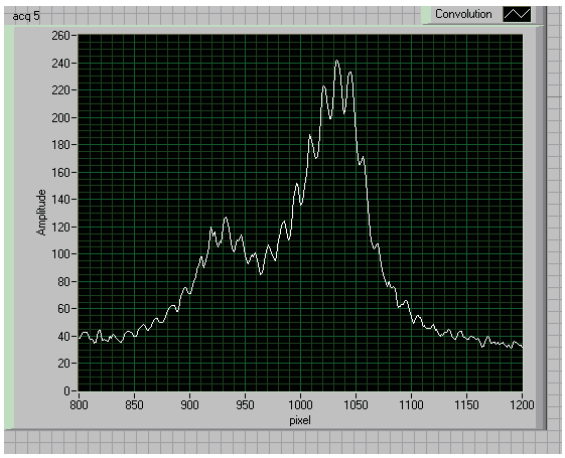

Fig. 6. Piston sensor spectrum, superposed with interference fringes. The density of the fringes increases with increasing piston.

The intensity distribution of the light on the camera can be written for one wavelength:

$$I(x) = I_0\left[1+\gamma\cos\left(\phi(x)\right)\right] \quad (1)$$

Where I(x) is the measured intensity distribution at the considered pixel x, γ is the contrast function and $\phi(x)$ is the phase between the two beams.
The phase term is directly proportional to the piston:

$$\phi(x) = \frac{2\pi P}{\lambda(x)} + \phi_0 \quad (2)$$

$\lambda(x) = \lambda_0 + k\,x$ is the wavelength and P is the piston.

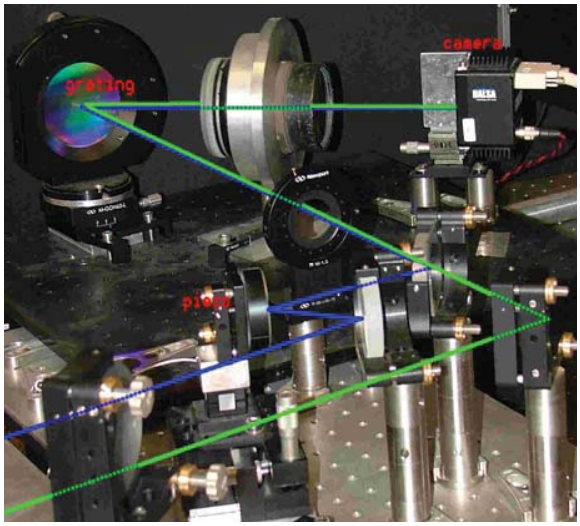

Fig. 7. Piston sensor hardware.

By comparing the phase term at two extreme wavelengths, the piston is computed:

$$P = \frac{\lambda(x_1)\lambda(x_2)}{2\pi}\,\frac{\phi(x_1)-\phi(x_2)}{\lambda(x_2)-\lambda(x_1)} \quad (3)$$

In order to measure the phase term for each corresponding wavelength, a phase shift algorithm is used by the acquisition of four intensity distributions with a fixed phase variation between the two beams.
The resulting phase term is given by the formula for unknown, but equal phase-shifts (Carré algorithm) [5].
The quality of the phase measurement in each point is evaluated with the fringe visibility.
The phase computed is still modulo 2π. A standard phase unwrapping is then necessary.
In conclusions, with four phase-shifted acquisitions, a phase term is computed for each pixel (corresponding to one wavelength). By comparing couple of phase terms from extreme wavelengths, one computes the piston between the two beams.
The RMS repeatability per measurement point is 2 µm over the range of (-3 mm to 3 mm). The standard deviation is 15 µm (-1.5 mm to 1.5 mm) and 25 µm (-3 mm to 3 mm).
A modulation threshold of 0.05 was set to accept the measurements.

In order to be as much as possible insensitive to vibrations and amplitude fluctuations of the source, the phase shift voltage was set to 0.25 V (about π/6) and delay of 25 ms was set before the acquisition.
Fig. 8 shows the piston calibration curve obtained with the previous settings. Near a zero piston, one becomes very sensitive to the phase measurement noise. The piston correction is limited by this noise 15 µm RMS.

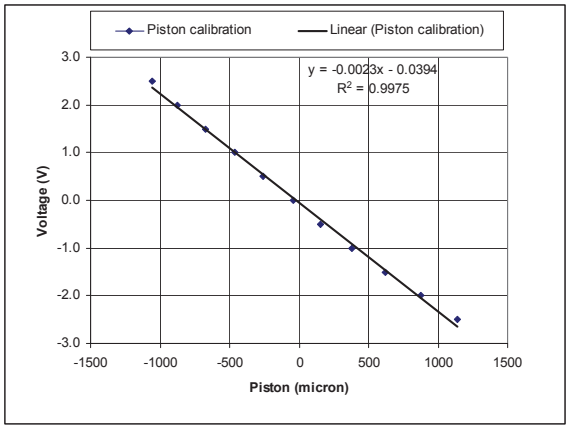

Fig. 8. Piston calibration in open loop; Voltage applied to the delay line versus piston (measured with piston sensor).

The calibration of the delay line has shown that the piston actuation introduces a coupling with the tilt actuation. In order to maintain the pistons sensing possible and to perform open loop calibration one has to maintain an active tip/tilt control loop. Physically speaking it means that two PSF need to remain overlapped to measure interference fringes. The use of the tip/tilt control loop is mandatory for a good operation of the piston sensor calibration.
The open loop dynamic range is ±1.2 mm. It is limited in dynamic range because of loss of contrast for piston above 1.2 mm. This loss of contrast is due to the fuzzy fringes sensed by the piston sensor combined with high fringe density. The fuzzy fringes appear because of the continuous compensation of the piston loop with a resolution of 250 nm. The latter acts as a phase-shift noise.
An original approach is used to circumvent this drawback, but limiting the number of acquisitions to 1 frame.
The alternative piston-sensing algorithm is based on a Fourier transform.
The spectrum is sampled in a uniform scheme along the axis of the frequency of light:

$$\phi(x)=\frac{2\pi P.\nu(x)}{c}+\phi_0 \qquad (4)$$

The piston is the "frequency" carrier in the spectrogram. The phase term is directly proportional to the time delay τ:

$$\phi(x)=2\pi\tau.\nu(x)+\phi_0 \qquad (5)$$

The Fourier transform (from light frequency-domain to time-domain) of a modulated flat light spectrum gives a single peak, which corresponds to the time delay τ). Using an appropriate over-sampling of the interferogram and a centroidisation algorithm in the Fourier transform, one can detect the peak with a sub-pixel resolution.
Indeed the 2048 spectral pixels give a temporal resolution (expressed in optical path delay $P=c.\tau$) of 8.35 µm/pixel.

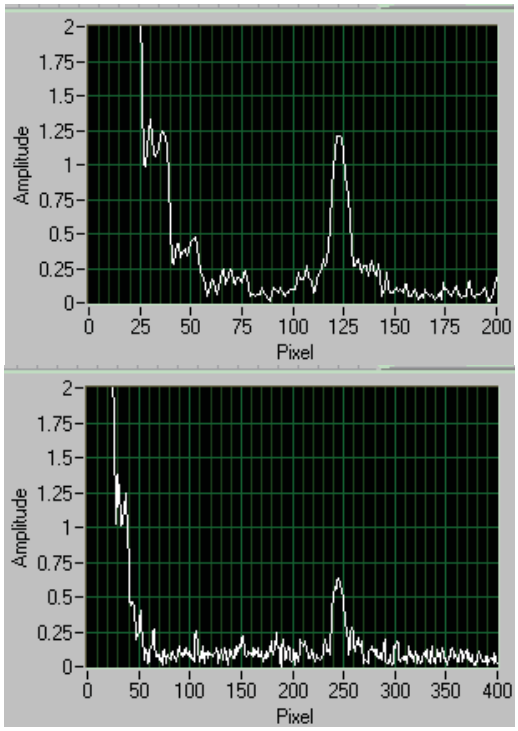

Fig. 9. Fourier Transform of interferogram. (Left) for small piston. (Right) For large piston.

The real frequency spectrum of our experiment is not flat. The lower part of the Fourier transforms (Fig. 9) need to be discriminated (typically 40 pixels or 335 µm). Fig. 10 shows a calibration of the Fourier transform piston, and confirms the excellent correlation between both methods. Table 6 gives a detailed comparison of the performance of both methods.
The Fourier transform method can be used as complementary method and back-up method to the Phase shifting algorithm.
The piston control loop contains several features to ensure its good operations. The piston measurement algorithm is itself a part of the measurement loop.
The algorithm makes two consecutive (valid) piston measurements before taking an action.
One observed that because of small drifts in the delay line the sign of the correction could be wrong. This is inherent to the phase shifting process.

Therefore, one implemented a verification/correction loop in the main loop. The closed piston loop stability has been characterised around a set point (zero piston) with an interferometric distancemeter. The temporal evolution of optical path length of the sample beam was monitored (Fig. 11).

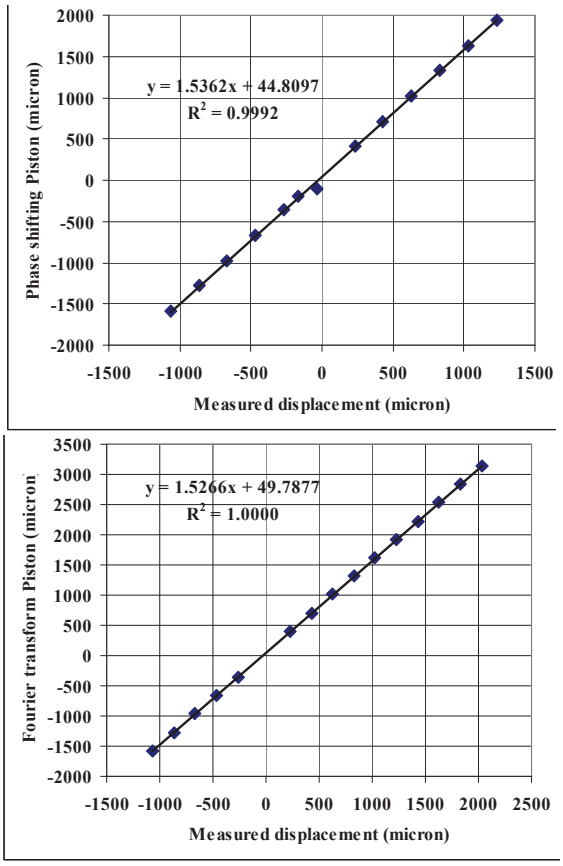

Fig. 10. Comparison between Phase shifting and Fourier transform Piston measurement.

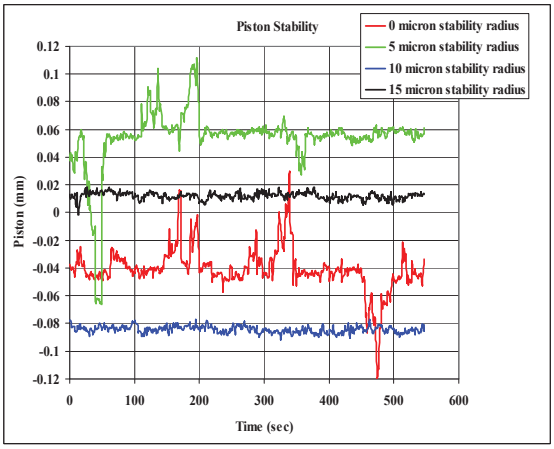

Fig. 11. Temporal evolution around the set point of 0 µm, for different stability radii of piston filter. An artificial offset has been added to the plots for better readability.

Characteristics	Phase shifting	Fourier transform
Range	-3 mm ... 3 mm (limited by the fringe stability)	0.4 mm ... 4.0 mm (lower bound limited by the source spectrum)
Repeatability	0.002 mm (with pass / fail criteria)	0.005 mm
Accuracy	0.025 mm (photon noise limited)	0.025 mm (photon noise limited)
Resolution around zero piston	0.025 mm	0.4 mm (limited by the source spectrum, it is possible to go down to 0.2 mm when subtracting a reference source spectrum)
Sign ambiguity (positive, negative piston)	No (resolved by the phase shifting method, but it is subject to stability of the interferogram)	Yes (a second measurement is needed, for example, measurement of the slope by applying a small displacement to the delay line)
Measurement time	140 msec (for an accepted measurement)	6 msec (all measurements are accepted)

Table 6: Comparison between Phase shifting and Fourier transform Piston measurement.

Stability radius (µm)	0	5	10	15
Piston RMS (mm)	0.015	0.021	0.003	0.003

Table 3: Piston stability for different stability radii of piston filter.

Different runs have been performed with a variation of the stability radius of a piston filter. Indeed when this filter is set to zero, every measurement is corrected including the piston sensor noise. The RMS piston is then of the order of the RMS piston sensor. With the introduction of the piston filter, we stabilize the closed loop operation especially around the 0 µm set point.

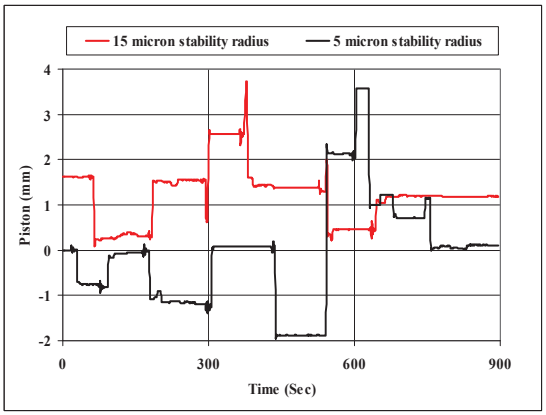

Fig. 12. Temporal evolution of the delay line. Two runs were performed with different stability radii of the piston filter.

Fig. 12 shows the temporal evolution of the delay line for different pistons. Two runs were performed with different stability radii of the piston filter. The perturbations are different in both runs.
Those plots show typically the sign error that appears as an overshoot which are typical in our phase-shifting algorithm: For example in the red plot: at times T=300 sec, T= 400 sec, and T= 500 sec, back plot at T= 600 sec.
One observes also small oscillatory behaviour before the jump, this is the result of the operator reaction with the optical bench. The delay line compensates these perturbations.

8. CONCLUSIONS

A complete active closed loop for piston and tip/tilt has been demonstrated. Piston and tip/ tilt sensing use an external incoherent light source, as a common absolute reference wave to the two interferometer arms.
The tip/tilt sensing loop that integrates the MICROMEGA DYNAMICS delay line, meets the expected performances: 1 mrad range, 0.01 mrad resolution.
The piston sensor operation is limited in dynamic range (limited by resolving power of the detector, fringe contrast) and resolution.
The piston sensor and delay line have been integrated in the loop. Due to coupling between tilt and piston actuation, it became quickly obvious that the piston loop can only operate and be characterised with the tip/tilt loop being closed.
Using adequate algorithms and pass/fail criteria on the piston measurement one has closed the piston loop and confirmed that the closed loop operation are limited by the piston sensor performances: 3 mm range, 0.025 mm resolution, 0.002 mm repeatability.
The breadboard demonstrator has an inherent drawback: its source was not adequate and not representative for an Earth spectrum. The current XENON-source has an important spectral spike in the spectral range of the piston sensor. This source problem highlights the criticality of the radiometric budget of the flight instrument.
The white light interferometer of the piston sensor processes the interferogram information with a phase shifting approach, which requires to have 4 stable interferograms (for given integration times of the camera). This is obviously in contradiction with the fact that the closed loop operation is not a stable environment. In the case of low light fluxes, one will increase the integration time of the frames; this can make phase-shifting interferometry impossible to work.

Improvements are:

-increase the flux on the detector using a cylindrical imaging lens that will integrate the light in the vertical axis on the detector pixels
-piston processing based on single measurements with Fourier analysis
-replace the bulk optics with optical fiber components and integrated optics (Y-coupler, phase-modulator)

9. ACKNOWLEDGMENTS

This work was funded by the Walloon Government (DGTRE/RW) in the framework of the European EUCLID programme. CSL acknowledges Maj. W. Tack (Belgian Army), ALENIA (Italy) and INETI (Portugal) for the continuous interest in this EUCLID programme.

10. REFERENCE DOCUMENTS

[1] B. Sorrente *et al.*, “Multiple-aperture optical telescopes: co-phasing sensor test-bed”. *5th International Conference On Space Optics*, volume SP-554, Toulouse, France, 2004. CNES/ESA, ESA.
[2] L. Mugnier et *al.*, “Multiple-aperture optical telescopes: some key issues for Earth observation from a GEO orbit”. *5th International Conference On Space Optics*, volume SP-554, Toulouse, France, 2004. CNES/ESA, ESA.
[3] F. Cassaing *et al.* “Optical design of a Michelson wide-field multi-aperture telescope”. *Optical System Design*, Saint-Etienne, France, 2003. Proc. Soc. Photo-Opt. Instrum. Eng, volume 5249.
[4] F.Shi *et al.*, Segmented mirror coarse phasing with white light interferometry : Modeling and Experiment on NGST’s wavefront Control testbed., NGST-ARTL-001882,
http://www.ngst.nasa.gov/hardware/text/WCT.html
(2000).
[5] D. Malacara, Optical shop testing, Second edition, J. Wiley & Sons, (1992).
[6] Statistical Optics, J.W. Goodman, Ed. John Wiley-Interscience (1985).